J Math Imaging Vis (2014) 49:273–288
DOI 10.1007/s10851-013-0459-y

Parameter Identification in Photothermal Imaging

A. Carpio · M.-L. Rapún

Published online: 10 September 2013
© Springer Science+Business Media New York 2013

Abstract We propose a technique to reconstruct the geometry of inclusions and their material parameters in thermal scattering near surfaces. The imaging problem is reformulated as a constrained optimization problem with a finite number of stationary constraints. The unknown domains and their parameters are the design variables. A descent method combining topological derivative analysis to find improved guesses of the objects and gradient iterations to correct their material parameters provides reasonable reconstructions.

Keywords Shape reconstruction · Parameter identification · Nondestructive testing · Topological derivative · Laplace transform · Heat equation · Thermal waves

1 Imaging Methods Using Thermal Waves

Photothermal imaging aims to reconstruct the inner structure of materials by heating their surface using a laser beam and recording the surface temperature. This procedure is expected to provide information on the distribution of defects or inclusions near the surface, regarding both their geometry (location, shape, orientation, size) and nature (physical parameters). Thermal waves are strongly damped. This fact restricts their application to superficial problems. Experiments [12, 23, 26, 27] suggest that photothermal techniques might become a valuable instrument in nondestructive testing of composite materials. In [22], the shape of an inhomogeneity in a turbid medium is reconstructed by tomographic techniques using thermal waves. Unknown fragments of a domain are determined from temperature measurements in a known region in [3, 4, 15]. Topological derivative techniques involving thermal waves are applied to domain identification in [7]. Dielectric coating factors and corrosion functions are calculated in [5, 16]. Theoretical results on inverse problems involving heat equations can be found in [10, 18]. The properties and usages of thermal waves are examined in [2, 20, 21, 25].

In this paper, we develop a technique to identify the material parameters and the geometry of inclusions by combining topological derivative methods and gradient strategies. Topological derivative techniques have been used to reconstruct the geometry of objects buried in a medium by means of acoustic scattering in a number of papers, see [6, 11, 13, 14] for instance. Incident waves are assumed to be time harmonic. This allows to reformulate the inverse problem as a constrained optimization problem, with stationary constraints for the stationary amplitudes of the waves. In photothermal imaging, incident thermal waves are usually pulse-like, not time harmonic. The resulting cost functionals have time dependent constraints. Different strategies to handle this difficulty were analyzed in [7], concluding that topological derivatives applied to an approximated Laplace transformed functional involving a finite number of stationary constraints were a promising procedure to reconstruct geometries. Here, we improve this technique to identify not only the buried domains but also their physical parameters. The idea is to combine topological derivative optimization to approximate the shape of the inclusions with gradient strategies to identify their parameters. Gradient techniques have

A. Carpio
Dept. Matemática Aplicada,
Universidad Complutense de Madrid, Madrid, Spain
e-mail: ana_carpio@mat.ucm.es

M.-L. Rapún (✉)
Dept. Fundamentos Matemáticos, ETSI Aeronáuticos,
Universidad Politécnica de Madrid, Madrid, Spain
e-mail: marialuisa.rapun@upm.es

been applied successfully in acoustic scattering and electric impedance tomography [6, 8]. Topological derivatives are combined with other kinds of minimization in [1].

The paper is organized as follows. Section 2 describes the inverse scattering problem for thermal waves in a half-space. Section 3 presents an approximated variational reformulation with a finite number of stationary constraints. Section 4 explains the hybrid topological derivative-gradient based technique to reconstruct domains and parameters. A formula for the corrections of the parameters in successive iterations in given. Finally, Sect. 5 illustrates the performance of the method in selected tests.

2 The Time Dependent Inverse Scattering Problem

We consider a matrix $\mathcal{R}$ containing inclusions Ω of a different material near its surface. This composite medium is identified with $\mathbb{R}^n_- := \{(x_1, \ldots, x_n) \in \mathbb{R}^n,\ x_n \leq 0\}$, $n = 2$ or 3. The surface of the sample $\Pi := \{(x_1, \ldots, x_n) \in \mathbb{R}^n,\ x_n = 0\}$ is thermically excited by an incident radiation U_{inc}. The goal is to determine the geometry and location of the inclusions in this semi–infinite medium from the temperature measured over a time interval on the surface Π.

The temperature of the system is governed by a transmission problem for the heat equation:

$$\begin{cases} U_t - \kappa_e \Delta U = 0, & \text{in } \mathcal{R} \times (0,\infty), \\ U_t - \kappa_i \Delta U = 0, & \text{in } \Omega \times (0,\infty), \\ U^- - U^+ = U_{inc}, & \text{on } \Gamma \times (0,\infty), \\ \partial_{\mathbf{n}} U^- - \partial_{\mathbf{n}} U^+ = \partial_{\mathbf{n}} U_{inc}, & \text{on } \Gamma \times (0,\infty), \\ \partial_{\mathbf{n}} U = 0, & \text{on } \Pi \times (0,\infty), \\ U(\cdot, 0) = 0, & \text{in } \mathbb{R}^n_-, \end{cases} \tag{1}$$

where $\mathcal{R} = \mathbb{R}^n_- \setminus \overline{\Omega}$. Here U represents the scattered field in $\mathcal{R}$ and the transmitted field in Ω. The outward normal vector $\mathbf{n}$ points outside $\mathcal{R}$. The superscripts "+" and "−" denote exterior and interior limiting values respectively. $\partial_{\mathbf{n}}$ stands for the normal derivative, with the normal vector pointing outside $\mathcal{R}$. The domain $\Omega \subset \mathbb{R}^n_-$ is an open bounded set with smooth boundary $\Gamma := \partial\Omega$. There may be an unknown number of unconnected components, that is, $\Omega = \bigcup_{j=1}^d \Omega_j$ with Ω_j open connected bounded sets satisfying $\overline{\Omega_l} \cap \overline{\Omega}_j = \emptyset$ for $l \neq j$ (see Fig. 1). The diffusivities of the background matrix and the inclusions are κ_e, $\kappa_i > 0$. We assume that κ_e is constant and that κ_i is a piecewise constant function attaining a possibly different constant value inside each component Ω_j of Ω. The transmission boundary condition for the normals sets the ratio between thermal conductivities equal to one for simplicity. The general case in which the conductivities are different involves the determination of two unknown parameters. This problem will be handled later in Sect. 4.3.

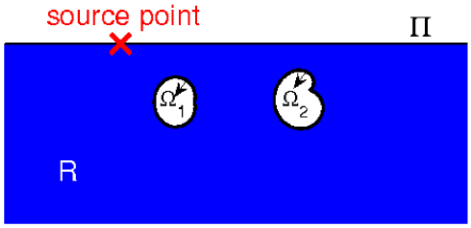

Fig. 1 Geometrical configuration: $\Omega = \bigcup_{j=1}^d \Omega_j$ and $\mathcal{R} = \mathbb{R}^n_- \setminus \overline{\Omega}$

The incident waves are time-dependent excitations of the form

$$U_{inc}(\mathbf{x}, t) = \frac{1}{t^{\frac{n}{2}}} \exp\left(-\frac{|\mathbf{x} - \mathbf{x}_0|^2}{4\kappa_e t}\right), \quad \mathbf{x} \in \mathbb{R}^n,\ \ t > 0, \tag{2}$$

which represent a point source placed at $\mathbf{x}_0$. We will locate the source point $\mathbf{x}_0$ on Π (see Fig. 1). The fact that all incoming heat to the domain is that of the source heating is modeled as the adiabaticity condition $\partial_{\mathbf{n}} U = 0$, on $\Pi \times (0,\infty)$. Notice that the incident waves (2) satisfy such condition for $\mathbf{x}_0 \in \Pi$.

In practice, the total temperature field is measured on a set of detectors Γ_{meas} placed on Π for different sampling times. The inverse problem consists in finding the structure and material constants of the obstacle Ω such that the solution of the forward transmission problem (1) equals the measured values $U_{meas}(\mathbf{x}, t_j)$ at the detector locations at times $t_1, \ldots, t_N$. Since this problem is ill-posed, we consider a weaker variational reformulation: Find Ω, κ_i minimizing

$$J(\mathcal{R}, \kappa_i) = \frac{1}{2} \sum_{j=1}^{N} f(t_j) \int_{\Gamma_{meas}} \big(U_{total}(\mathbf{x}, t_j) - U_{meas}(\mathbf{x}, t_j)\big)^2 dl_{\mathbf{x}},$$

when $U_{total}(\mathbf{x}, t) = U(\mathbf{x}, t) + U_{inc}(\mathbf{x}, t)\chi_{\mathcal{R}}(\mathbf{x})$. Here, $U(\mathbf{x}, t)$ stands for the solution of the forward problem (1), which acts as a constraint. $\chi_{\mathcal{R}}(\mathbf{x})$ is the characteristic function of the domain $\mathcal{R} = \mathbb{R}^n_- \setminus \overline{\Omega}$, satisfying $\chi_{\mathcal{R}} = 1$ on Γ_{meas}.

The weight function $f(t) > 0$ normalizes the time decay of solutions of the heat equation. The incident waves (2) are positive functions decaying with time. For $\mathbf{x} \neq \mathbf{x}_0$, they start from $U_{inc}(\mathbf{x}, 0) = 0$, reach a maximum at $t = |\mathbf{x} - \mathbf{x}_0|^2/(4\kappa_e n)$ and then decrease to zero as time increases. Solutions U of (1) decay in a similar way. Different choices for f are discussed when presenting the numerical results.

3 Approximated Cost Functional

The original optimization problem with time-dependent constraints is replaced by a problem with stationary constraints using Laplace transforms. This is done in several steps, described below.

3.1 Extension to the Whole Space

The first step in the process consists in extending the constraint to the whole space by reflection using the boundary condition at the interface Π. This avoids to deal explicitly with this condition and provides a simpler variational formulation of the stationary problems that appear after performing Laplace transforms. We denote by $\widehat{\mathbf{x}}$ the reflected point of $\mathbf{x}$ with respect to Π, that is, $\widehat{\mathbf{x}} = (x_1, x_2, -x_3)$ for $\mathbf{x} = (x_1, x_2, x_3) \in \mathbb{R}^3$ or $\widehat{\mathbf{x}} = (x_1, -x_2)$ for $\mathbf{x} = (x_1, x_2) \in \mathbb{R}^2$. Then, we consider the symmetric domains

$$\widetilde{\Omega} := \Omega \cup \{\mathbf{x} \in \mathbb{R}^n,\ \widehat{\mathbf{x}} \in \Omega\}, \quad \widetilde{\mathcal{R}} := \mathbb{R}^n \setminus \overline{\widetilde{\Omega}},$$

and $\widetilde{\Gamma} := \Gamma \cup \{\mathbf{x} \in \mathbb{R}^n,\ \widehat{\mathbf{x}} \in \Gamma\}$. If $U(\mathbf{x}, t)$ solves (1), the reflected function

$$\widetilde{U}(\mathbf{x}, t) := \begin{cases} U(\mathbf{x}, t), & \text{if } \mathbf{x} \in \mathbb{R}^n_-, \\ U(\widehat{\mathbf{x}}, t), & \text{if } \mathbf{x} \in \mathbb{R}^n \setminus \mathbb{R}^n_-, \end{cases}$$

verifies

$$\begin{cases} \widetilde{U}_t - \kappa_e \Delta \widetilde{U} = 0, & \text{in } \widetilde{\mathcal{R}} \times (0, \infty), \\ \widetilde{U}_t - \kappa_i \Delta \widetilde{U} = 0, & \text{in } \widetilde{\Omega} \times (0, \infty), \\ \widetilde{U}^- - \widetilde{U}^+ = \widetilde{U}_{inc}, & \text{on } \widetilde{\Gamma} \times (0, \infty), \\ \partial_{\mathbf{n}} \widetilde{U}^- - \partial_{\mathbf{n}} \widetilde{U}^+ = \partial_{\mathbf{n}} \widetilde{U}_{inc}, & \text{on } \widetilde{\Gamma} \times (0, \infty), \\ \widetilde{U}(\cdot, 0) = 0, & \text{in } \mathbb{R}^n, \end{cases} \tag{3}$$

where

$$\widetilde{U}_{inc}(\mathbf{x}, t) := \begin{cases} U_{inc}(\mathbf{x}, t), & \text{if } \mathbf{x} \in \mathbb{R}^n_-, \\ U_{inc}(\widehat{\mathbf{x}}, t), & \text{if } \mathbf{x} \in \mathbb{R}^n \setminus \mathbb{R}^n_-. \end{cases} \tag{4}$$

Reciprocally, if $\widetilde{U}$ is a solution of (3), symmetry implies that $U := \widetilde{U}$ in $\mathbb{R}^n_-$ is a solution of (1).

The extended optimization problem is then: find Ω and κ_i minimizing the functional

$$J(\widetilde{\mathcal{R}}, \kappa_i) := \frac{1}{2} \sum_{j=1}^{N} f(t_j) \int_{\Gamma_{meas}} \big(\widetilde{U}_{total}(\mathbf{x}, t_j) - \widetilde{U}_{meas}(\mathbf{x}, t_j)\big)^2 dl_{\mathbf{x}}, \tag{5}$$

when $\widetilde{U}_{total}(\mathbf{x}, t) = \widetilde{U}(\mathbf{x}, t) + \widetilde{U}_{inc}(\mathbf{x}, t)\chi_{\widetilde{\mathcal{R}}}(\mathbf{x})$.

For ease of notation, from now on U will denote either the solution of (1) or (3) and we will omit the tildes for $\widetilde{\mathcal{R}}$, $\widetilde{\Omega}$ and $\widetilde{\Gamma}$.

3.2 Laplace Transformed Problem

The second step consists in applying Laplace transforms to generate the stationary constraints. Let U_{inc} be the incident wave defined in (2)–(4) and U the solution of the extended time-dependent forward problem (3). We define now u_{inc} and u as the Laplace transforms in time of U_{inc} and U:

$$u_{inc}(\mathbf{x}, s) = \int_0^\infty e^{-st} U_{inc}(\mathbf{x}, t)\, dt,$$

$$u(\mathbf{x}, s) = \int_0^\infty e^{-st} U(\mathbf{x}, t)\, dt, \quad \mathbf{x} \in \mathbb{R}^n.$$

For each s, the function $u_s(\mathbf{x}) := u(\mathbf{x}, s)$ is a solution of

$$\begin{cases} \Delta u_s + \lambda_{s,e}^2 u_s = 0, & \text{in } \mathcal{R}, \\ \Delta u_s + \lambda_{s,i}^2 u_s = 0, & \text{in } \Omega, \\ u_s^- - u_s^+ = u_{inc,s}, & \text{on } \Gamma, \\ \partial_{\mathbf{n}} u_s^- - \partial_{\mathbf{n}} u_s^+ = \partial_{\mathbf{n}} u_{inc,s}, & \text{on } \Gamma, \end{cases} \tag{6}$$

with $\lambda_{s,e}^2 := -s/\kappa_e$, $\lambda_{s,i}^2 := -s/\kappa_i$ and $u_{inc,s}(\mathbf{x}) := u_{inc}(\mathbf{x}, s)$. The Laplace transforms of the incident fields (2) are:

$$u_{inc}(\mathbf{x}, s) = \begin{cases} 2K_0(|\mathbf{x} - \mathbf{x}_0|\sqrt{s/\kappa_e}), & \text{if } n = 2, \\ \frac{2\sqrt{\pi\kappa_e}}{|\mathbf{x}-\mathbf{x}_0|} \exp(-|\mathbf{x} - \mathbf{x}_0|\sqrt{s/\kappa_e}), & \text{if } n = 3, \end{cases} \tag{7}$$

K_0 being the modified Bessel function of order zero. These expressions hold for $\mathbf{x} \in \mathbb{R}^n$, $\mathrm{Re}(s) > 0$, and can be holomorphically extended to $s \in \mathbb{C} \setminus (-\infty, 0]$ (see [17, Lemma 10]).

Problem (6) is a stationary transmission problem for the Helmholtz equation that has a unique solution verifying the Sommerfeld radiation condition at infinity,

$$\lim_{r \to \infty} r^{(n-1)/2} (\partial_r u_s - \imath \lambda_{s,e} u_s) = 0, \quad r = |\mathbf{x}|, \tag{8}$$

for all $s \in \mathbb{C} \setminus (-\infty, 0]$ (see [9, Proposition 4.7]). This characterization of $u_s(\mathbf{x})$ defines $u(\cdot, s)$ for all $s \in \mathbb{C} \setminus (-\infty, 0]$ as an holomorphic function of s.

Inverting the Laplace transform, we recover the solution of the time-dependent problem (3):

$$U(\mathbf{x}, t) = \frac{1}{2\pi\imath} \int_{\mathcal{C}} e^{st}\, u(\mathbf{x}, s)\, ds.$$

To invert the Laplace transform we must solve (6)–(8) for $s \in \mathcal{C}$. From a computational standpoint, the best inversion paths $\mathcal{C}$ are those along which the resulting integral can be sharply approximated by a quadrature formula involving few nodes. We use the hyperbolic paths proposed in [19], parametrized by $\gamma : \mathbb{R} \to \mathcal{C}$ where

$$\gamma(\theta) := \mu\big(1 - \sin(\beta + \imath\theta)\big), \quad \theta \in \mathbb{R},$$

with $\mu > 0$ and $0 < \beta < \pi/2$. Then, U is given by:

$$U(\mathbf{x}, t) = \frac{1}{2\pi\imath} \int_{-\infty}^{\infty} e^{\gamma(\theta)t} u\big(\mathbf{x}, \gamma(\theta)\big)\, \gamma'(\theta)\, d\theta. \tag{9}$$

In our numerical tests $\beta = \pi/4$ and μ is selected depending on the values of t, in such a way that $\mu \approx 5/t$, see [17] for

technical details and a proof of the fact that Laplace inversion formulae work for our transmission problem (3).

The transformed cost functional (5) becomes:

$$J(\mathcal{R},\kappa_i) = \frac{1}{2}\sum_{j=1}^{N} f(t_j)\int_{\Gamma_{meas}} \big(U_{total}(\mathbf{x},t_j) - U_{meas}(\mathbf{x},t_j)\big)^2 dl_{\mathbf{x}}$$
$$= \frac{1}{2}\sum_{j=1}^{N} f(t_j)\int_{\Gamma_{meas}} \left| \int_{-\infty}^{\infty} e^{\gamma(\theta)t_j} u_{total,\gamma(\theta)}(\mathbf{x}) \times \frac{\gamma'(\theta)}{2\pi\imath} d\theta - U_{meas}(\mathbf{x},t_j)\right|^2 dl_{\mathbf{x}}. \tag{10}$$

Here, $u_{total,\gamma(\theta)}(\mathbf{x}) = u_{\gamma(\theta)}(\mathbf{x}) + u_{inc,\gamma(\theta)}(\mathbf{x})\chi_{\mathcal{R}}(\mathbf{x})$, with $u_{inc,\gamma(\theta)}(\mathbf{x}) = u_{inc}(\mathbf{x},\gamma(\theta))$ defined in (7) and $u_{\gamma(\theta)}$ the solution of (6)–(8) for $s=\gamma(\theta)$. The functions $U_{total}(\mathbf{x},t)$ and $U_{meas}(\mathbf{x},t)$ are real-valued. For each value of θ, $u_{total,\gamma(\theta)}(\mathbf{x})$ and the factors $e^{t_j\gamma(\theta)}$ and $\gamma'(\theta)$ are complex-valued.

3.3 Discretized Functional

The third step is to generate an approximate cost functional with a finite number of stationary constraints discretizing the integrals from $-\infty$ to ∞ using a truncated trapezoidal rule. We approximate the inversion formula (9) by:

$$U(\mathbf{x},t) \sim \sum_{\ell=-m}^{m} c_\ell\, e^{s_\ell t} u(\mathbf{x},s_\ell), \tag{11}$$

with nodes and weights

$$s_\ell := \gamma\left(\frac{\log(m)}{m}\,\ell\right), \qquad c_\ell := \frac{\log(m)}{2\pi\imath m}\,\gamma'\left(\frac{\log(m)}{m}\,\ell\right),$$

where $u(\mathbf{x},s_\ell) = u_{s_\ell}(\mathbf{x})$ is the solution of problem (6)–(8) with $s=s_\ell$. By symmetry, we only need to solve $m+1$ stationary problems because $u(\cdot,\overline{s_\ell})$ is computed using $u(\cdot,s_\ell)$. For the selected hyperbolic paths, convergence is exponential in m and few nodes are needed (about 10 suffice). Once m is selected and $u_{s_\ell}(\mathbf{x})$ is evaluated, formula (11) can be used to compute $U(\mathbf{x},t)$ for different values of t in the time interval under study.

The Laplace transformed cost functional (10) is approximated as

$$J(\mathcal{R},\kappa_i) := \frac{1}{2}\sum_{j=1}^{N} f(t_j)\int_{\Gamma_{meas}} \left| \sum_{\ell=-m}^{m} c_\ell\, e^{s_\ell t_j} u_{total,s_\ell}(\mathbf{x};\kappa_i) - U_{meas}(\mathbf{x},t_j)\right|^2 dl_{\mathbf{x}}, \tag{12}$$

where

$$u_{total,s_\ell}(\mathbf{x};\kappa_i) = \begin{cases} u_{inc,s_\ell}(\mathbf{x}) + u_{s_\ell}(\mathbf{x};\kappa_i), & \text{in } \mathcal{R},\\ u_{s_\ell}(\mathbf{x};\kappa_i), & \text{in } \Omega, \end{cases} \tag{13}$$

with $u_{inc,s_\ell}(\mathbf{x}) = u_{inc}(\mathbf{x},s_\ell)$ defined in (7) and u_{s_ℓ} a solution of (6)–(8) with $\lambda_{s,e}^2 = -s_\ell/\kappa_e$ and $\lambda_{s,i}^2 = -s_\ell/\kappa_i$. This approximate optimization problem has $2m+1$ stationary restrictions (6)–(8), that are reduced to $m+1$ forward stationary problems by symmetry.

4 Hybrid Technique to Reconstruct Objects and Parameters

The optimization problem of finding Ω and κ_i minimizing the functional (12) can be solved combining gradient and topological derivative methods. Once a first approximation for the domains and their parameters is selected, we generate sequences of corrected domains and parameters in such a way that the cost functional decreases. At each stage, the guess for the domains is fixed and the parameters are modified using correctors calculated with a gradient method. Then, the current guesses for the parameters are fixed whereas the approximated domains are updated computing the topological derivative of the resulting cost functional. The algorithm alternates a few gradient iterations to correct the parameter values with a topological derivative computation to update the domains.

4.1 Gradient Iteration for the Parameters

If we fix the inclusions Ω, the functional (12) depends only on the coefficient κ_i. Given a guess $\kappa_{i,q}$ we look for a correction $\kappa_{i,q+1} = \kappa_{i,q} + \eta\psi$, with $\eta\in\mathbb{R}$, selecting ψ in such a way that the functional decreases for small η. We assume here that κ_i is a piecewise constant parameter, taking different constant values in different components of Ω. However, similar results can be established for smoothly varying κ replacing $\kappa\Delta u$ by $\operatorname{div}(\kappa\nabla u)$ in the heat equations, following [6, 8].

An expression for ψ is obtained evaluating the derivative of $J(\eta) = J(\mathcal{R},\kappa_{i,q}+\eta\psi)$, where the functional J is defined in (12). By linearity, we can consider independently each value $t=t_j$ in J. Then, we add the different contributions to get the final formula. In this way, the sought result will follow as a corollary of the following theorem by superposition.

Theorem 1 *The derivative with respect to η of the function*

$$G(\eta,t) := \frac{1}{2}\int_{\Gamma_{meas}} \left| \sum_{\ell=-m}^{m} c_\ell\, e^{s_\ell t} u_{total,s_\ell}(\mathbf{x};\kappa_i+\eta\psi) - U_{meas}(\mathbf{x},t)\right|^2 dl_{\mathbf{x}}$$

evaluated at $\eta = 0$ is

$$\frac{\partial}{\partial \eta} G(0,t) = \mathrm{Re}\left(\sum_{\ell=-m}^{m} \int_{\Omega} \frac{s_\ell}{\kappa_i^2}\, \psi\, u_{total,s_\ell}(\mathbf{x};\kappa_i)\, p_{s_\ell}(\mathbf{x},t) d\mathbf{x} \right)$$

where the adjoint field $p_{s_\ell}(\mathbf{x},t)$ is the solution of

$$\begin{cases} \Delta p + \lambda_{s_\ell,e}^2\, p = B_\ell\, \delta_{\Gamma_{meas}}, & \text{in } \mathcal{R}, \\ \Delta p + \lambda_{s_\ell,i}^2\, p = 0, & \text{in } \Omega, \\ p^- - p^+ = 0, & \text{on } \Gamma, \\ \partial_{\mathbf{n}} p^- - \partial_{\mathbf{n}} p^+ = 0, & \text{on } \Gamma, \\ \lim_{r\to\infty} r^{(n-1)/2}(\partial_r p - \imath \lambda_{s_\ell,e} p) = 0, & \end{cases} \tag{14}$$

with $\lambda_{s_\ell,e}^2 = -s_\ell/\kappa_e$ and $\lambda_{s_\ell,i}^2 = -s_\ell/\kappa_i$. Here

$$B_\ell(\mathbf{x},t) := c_\ell e^{s_\ell t} \left(\overline{U_{meas}(\mathbf{x},t) - \sum_{k=-m}^{m} c_k e^{t s_k} u_{total,s_k}(\mathbf{x};\kappa_i)} \right).$$

Proof Let us consider a large ball $B_R = B(0,R)$ containing Ω and Γ_{meas}, and set $\Gamma_R = \partial B_R$ and $\Omega_R = (\mathcal{R} \setminus \overline{\Omega}) \cap B_R$. Let $L(s)$ be the Dirichlet-to-Neumann operator on Γ_R associated to the equation $\Delta u - \frac{s}{\kappa_e} u = 0$ in the exterior of B_R. We define the sesquilinear form and the conjugate linear map:

$$\begin{aligned} b(\eta, s; u, w) := & \int_{\Omega_R} \left(\nabla u \nabla \overline{w} + \frac{s}{\kappa_e} u \overline{w} \right) d\mathbf{x} \\ & + \int_{\Omega} \left(\nabla u \nabla \overline{w} + \frac{s}{\kappa_i + \eta\psi} u \overline{w} \right) d\mathbf{x} \\ & - \int_{\Gamma_R} \big(L(s) u \big) \overline{w}\, dl, \end{aligned}$$

$$l(s; w) := \int_{\Gamma_R} \big(\partial_{\mathbf{n}} u_{inc,s} - L(s) u_{inc,s} \big) \overline{w}\, dl.$$

Let $N(\eta, s) = N(\eta, s; \mathbf{x}) \in H^1(B_R)$ be the solution of

$$b\big(\eta, s; N(\eta,s), w\big) = l(s; w), \quad \forall w \in H^1(B_R).$$

Notice that $N(\eta, s_\ell; \mathbf{x}) = u_{total,s_\ell}(\mathbf{x}; \kappa_i + \eta\psi)$ for $\ell = -m, \ldots, m$.

The derivative of the function $G(\eta, t)$ with respect to the parameter η is

$$\begin{aligned} & \frac{\partial}{\partial \eta} G(0,t) \\ & \quad = \mathrm{Re} \sum_{\ell=-m}^{m} c_\ell e^{s_\ell t} \left[\int_{\Gamma_{meas}} \overline{U_{diff}(\mathbf{x},t)} \frac{\partial}{\partial \eta} N(0, s_\ell; \mathbf{x}) dl_{\mathbf{x}} \right], \end{aligned}$$

where $U_{diff}(\mathbf{x},t) = \sum_{\ell=-m}^{m} c_\ell e^{s_\ell t} N(0, s_\ell; \mathbf{x}) - U_{meas}(\mathbf{x},t)$.

To avoid the computation of $\frac{\partial}{\partial \eta} N(0, s_\ell)$ we introduce the modified Lagrangian

$$\begin{aligned} & \mathcal{L}(\eta, t; \mathbf{u}, \mathbf{p}) \\ & \quad = G(\eta, t) - \mathrm{Re} \left[\sum_{\ell=-m}^{m} c_\ell e^{s_\ell t} \big(b(\eta, s_\ell; u_\ell, p_\ell) - l(s_\ell; p_\ell) \big) \right] \end{aligned}$$

for all $\mathbf{u} = (u_{-m}, \ldots, u_m)$, $\mathbf{p} = (p_{-m}, \ldots, p_m) \in (H^1(B_R))^{2m+1}$. Differentiating the identity

$$\begin{aligned} & G(\eta, t) = \mathcal{L}\big(\eta, t; \big(N(\eta, s_{-m}), \ldots, N(\eta, s_m)\big), \mathbf{p}\big) \\ & \quad \forall \mathbf{p} \in \big(H^1(B_R)\big)^{2m+1}, \end{aligned}$$

we find a more convenient expression for the derivative:

$$\begin{aligned} \frac{\partial}{\partial \eta} G(0,t) = \mathrm{Re} & \sum_{\ell=-m}^{m} c_\ell e^{s_\ell t} \\ & \times \left(\int_{\Gamma_{meas}} \overline{U_{diff}(\mathbf{x},t)} \frac{\partial}{\partial \eta} N(0, s_\ell; \mathbf{x}) dl_{\mathbf{x}} \right. \\ & - b\left(0, s_\ell; \frac{\partial}{\partial \eta} N(0, s_\ell), p_\ell \right) \\ & \left. + \int_{\Omega} \frac{s_\ell}{\kappa_i^2} \psi N(0, s_\ell; \mathbf{x}) \overline{p}_\ell(\mathbf{x}) d\mathbf{x} \right) \end{aligned} \tag{15}$$

whenever $\mathbf{p} \in (H^1(B_R))^{2m+1}$. If we select now $\mathbf{p} = (q(s_{-m}), \ldots, q(s_m))$ where $q(s) \in H^1(B_R)$ satisfies

$$b\big(0, s; v, q(s)\big) = \int_{\Gamma_{meas}} \overline{U_{diff}(\mathbf{x},t)} v(\mathbf{x}) dl_{\mathbf{x}}, \quad \forall v \in H^1(B_R),$$

the desired derivative is given by the last term in (15). Therefore,

$$\frac{\partial}{\partial \eta} G(0,t) = \mathrm{Re} \left(\sum_{\ell=-m}^{m} \int_{\Omega} \frac{s_\ell}{\kappa_i^2}\, \psi N(0, s_\ell) \big(c_\ell e^{s_\ell t} \overline{q}(s_\ell) \big) d\mathbf{x}. \right)$$

It is rather simple to show now that $p_{s_\ell} := c_\ell e^{s_\ell t} \overline{q}(s_\ell)$ is a solution of (14), which finishes the proof. □

As a corollary of the previous theorem, by superposition for several times t_j we find the derivative of the original function $J(\eta)$:

Corollary 1 *The derivative with respect to η of the function $J(\eta) := J(\mathcal{R}, \kappa_{i,q} + \eta\psi)$ at $\eta = 0$ is*

$$J'(0) = \mathrm{Re} \left(\sum_{\ell=-m}^{m} \int_{\Omega} \frac{s_\ell}{\kappa_{i,q}^2}\, \psi\, u_{total,s_\ell}(\mathbf{x};\kappa_{i,q})\, p_{s_\ell}(\mathbf{x})\, d\mathbf{x} \right)$$

where the adjoint field p_{s_ℓ} is the solution of

$$\begin{cases} \Delta p + \lambda^2_{s_\ell,e}\, p = B_\ell\, \delta_{\Gamma_{meas}}, & \text{in } \mathcal{R}, \\ \Delta p + \lambda^2_{s_\ell,i}\, p = 0, & \text{in } \Omega, \\ p^- - p^+ = 0, & \text{on } \Gamma, \\ \partial_{\mathbf{n}} p^- - \partial_{\mathbf{n}} p^+ = 0, & \text{on } \Gamma, \\ \lim_{r\to\infty} r^{(n-1)/2}(\partial_r p - \imath\lambda_{s_\ell,e} p) = 0, & \end{cases} \tag{16}$$

with $\lambda^2_{s_\ell,e} = -s_\ell/\kappa_e$ and $\lambda^2_{s_\ell,i} = -s_\ell/\kappa_{i,q}$. Here

$$B_\ell(\mathbf{x}) := \sum_{j=1}^{N} f(t_j) c_\ell e^{t_j s_\ell} \times \overline{\left(U_{meas}(\mathbf{x}, t_j) - \sum_{k=-m}^{m} c_k e^{t_j s_k} u_{total,s_k}(\mathbf{x}; \kappa_{i,q}) \right)}.$$

For fixed Ω, the descent direction for the diffusion coefficient can be chosen as:

$$\psi = -\operatorname{Re} \int_\Omega \left(\sum_{\ell=-m}^{m} s_\ell\, u_{total,s_\ell}(\mathbf{x}; \kappa_{i,q})\, p_{s_\ell}(\mathbf{x}) \right) d\mathbf{x}.$$

This choice makes it negative the expression for the derivative of $J'(0)$ given above.

When κ_i is a piecewise constant function attaining the value κ_i^j inside Ω_j (recall that $\Omega = \bigcup_{j=1}^d \Omega_j$), we look for a piecewise constant approximation. Given the guesses $\kappa_{i,q}^j$ for κ_i^j we correct them setting $k_{i,q+1}^j = k_{i,q}^j + \eta\psi_j$ with

$$\psi_j = -\operatorname{Re} \int_{\Omega_j} \left(\sum_{\ell=-m}^{m} s_\ell\, u_{total,s_\ell}\left(\mathbf{x}; \left(\kappa_{i,q}^1, \ldots, \kappa_{i,q}^d\right)\right) \times p_{s_\ell}(\mathbf{x}) \right) d\mathbf{x}, \tag{17}$$

where $u_{total,s_\ell}(\mathbf{x}; (\kappa_{i,q}^1, \ldots, \kappa_{i,q}^d))$ is defined as in (13) with $u_{s_\ell}(\mathbf{x}; (\kappa_{i,q}^1, \ldots, \kappa_{i,q}^d))$ a solution of (6)–(8) with $\lambda^2_{s,e} = -s_\ell/\kappa_e$ and $\lambda^2_{s,i} = -s_\ell/\kappa_{i,q}^j$ inside each Ω_j. The adjoint fields p_{s_ℓ} are defined likewise: they are solutions of (16) with $\lambda^2_{s,e} = -s_\ell/\kappa_e$ and $\lambda^2_{s,i} = -s_\ell/\kappa_{i,q}^j$ inside Ω_j.

4.2 Topological Derivative Iteration

When κ_i is fixed the functional (12) becomes just a shape functional. Its topological derivative allows to find first guesses of possible inclusions and improve them afterwards. The topological derivative of a shape functional $J(\mathcal{R})$ is a pointwise function defined at each $\mathbf{x} \in \mathcal{R}$:

$$D_T(\mathbf{x}, \mathcal{R}) = \lim_{\varepsilon\to 0} \frac{J(\mathcal{R} \setminus \overline{B_\varepsilon(\mathbf{x})}) - J(\mathcal{R})}{\text{Volume}(B_\varepsilon(\mathbf{x}))}, \quad \mathbf{x} \in \mathcal{R}, \tag{18}$$

for balls $B_\varepsilon(\mathbf{x})$ centered at $\mathbf{x}$ with radius ε. This yields the expansion:

$$J\left(\mathcal{R} \setminus \overline{B_\varepsilon(\mathbf{x})}\right) = J(\mathcal{R}) + D_T(\mathbf{x}, \mathcal{R}) \text{Volume}\left(B_\varepsilon(\mathbf{x})\right) + o\big(\text{Volume}\left(B_\varepsilon(\mathbf{x})\right)\big).$$

If we center $B_\varepsilon(\mathbf{x})$ at a point $\mathbf{x}$ where $D_T(\mathbf{x}, \mathcal{R})$ is negative, J decreases: $J(\mathcal{R} \setminus \overline{B_\varepsilon(\mathbf{x})}) < J(\mathcal{R})$. For our cost functional a guess for the location of the inclusions Ω is found taking Ω_0 to be a set of points with large negative topological derivatives. Given an approximation Ω_q, we may improve it by evaluating $D_T(\mathbf{x}, \mathbb{R}^n \setminus \overline{\Omega}_q)$ at $\mathbf{x} \in \mathbb{R}^n \setminus \overline{\Omega}_q$ and adding to Ω_q the points where it attains large negative values. This allows to correct the shapes and create new components [6]:

$$\Omega_{q+1} = \Omega_q \cup \left\{ \mathbf{x} \in \mathbb{R}^n \setminus \overline{\Omega}_q \mid D_T\left(\mathbf{x}, \mathbb{R}^n \setminus \overline{\Omega}_q\right) \le -C_q \right\} \tag{19}$$

for decreasing thresholds $C_q > 0$. This generates an increasing sequence of domains. If at some stage a spurious region is included, it cannot be removed. Spurious points included in a guess of the domains can be withdrawn with a modified notion of topological derivative exploited in [6]. The idea is to add to the current guess of the domains points where the topological derivative takes the larger negative values, and to remove points at which the values of the extended topological derivative becomes too large. The topological derivative of a functional $J(\mathbb{R}^n \setminus \overline{\Omega}_q)$ is extended to the points inside Ω_q as

$$D_T\left(\mathbf{x}, \mathbb{R}^n \setminus \overline{\Omega}_q\right) = \lim_{\varepsilon\to 0} \frac{J(\mathbb{R}^n \setminus \overline{\Omega}_q) - J(\mathbb{R}^n \setminus (\overline{\Omega_q \setminus B_\varepsilon(\mathbf{x})}))}{\text{Volume}(B_\varepsilon(\mathbf{x}))}, \quad \mathbf{x} \in \Omega_q. \tag{20}$$

A non-monotone sequence of objects is generated substituting the previous definition of Ω_{q+1} by:

$$\Omega_{q+1} = \Omega_q \cup \left\{ \mathbf{x} \in \mathbb{R}^n \setminus \overline{\Omega}_q \;\middle|\; D_T\left(\mathbf{x}, \mathbb{R}^n \setminus \overline{\Omega}_q\right) \le -C_q \right\} \setminus \overline{\left\{ \mathbf{x} \in \Omega_q \mid D_T\left(\mathbf{x}, \mathbb{R}^n \setminus \overline{\Omega}_q\right) \ge c_q \right\}}, \tag{21}$$

for decreasing sequences C_q, $c_q > 0$. The quality of the reconstructions, as well as the number of iterations depends on the values of the constants C_q and c_q. If they are "big", the number of iterations is higher, but it is more unlikely to include spurious points. For our numerical experiments we selected them following the guidelines in [6]. Originally C_q is chosen as the largest negative value of the topological derivative attained when $\Omega = \Omega_q$ multiplied by a factor $\delta_q < 1$. In principle we take $\delta_1 = 0.85$ and $\delta_q = 0.9$ for $q \ge 2$. The value of δ_q is accepted if the functional decreases in the next iteration. Otherwise, δ_q is increased. For c_q we proceed likewise and multiply by δ_q the largest positive value of the topological derivative attained at the interior of the object.

In practice, topological derivatives for functionals with stationary boundary value constraints are calculated using explicit expressions in terms of adjoint and forward fields. The following result provides a formula for the computation of the topological derivative.

Theorem 2 *For a fixed value of κ_i, the topological derivative of the cost functional (12) is given by*

$$D_T\left(\mathbf{x}, \mathbb{R}^n \setminus \overline{\Omega}_q\right) = \mathrm{Re}\left(\sum_{\ell=-m}^{m}\left(\frac{1}{\kappa_e}-\frac{1}{\kappa_i}\right) s_\ell\, u_{total,s_\ell}(\mathbf{x};\kappa_i)\, p_{s_\ell}(\mathbf{x})\right), \quad \mathbf{x}\in\mathbb{R}^n, \tag{22}$$

where u_{total,s_ℓ} and p_{s_ℓ} are defined as in (13) and (16) with domain $\Omega=\Omega_q$ and parameters $\lambda^2_{s_\ell,e}=-s_\ell/\kappa_e$ and $\lambda^2_{s_\ell,i}=-s_\ell/\kappa_i$.

Proof For a fixed piecewise constant κ_i the topological derivative of the functional (12) for $\mathbf{x}\in\mathbb{R}^n\setminus\overline{\Omega}_q$ was computed in [7] using the classical definition (18). The formula inside the objects using (20), that is, for $\mathbf{x}\in\Omega_q$, can be easily obtained combining the results in [6] and [7]. □

To implement formula (22) the parameter κ_i has to be defined for all $\mathbf{x}\in\mathbb{R}^n$. To compute $D_T(\mathbf{x},\mathbb{R}^n)$ we take a constant initial approximation $\kappa_{i,0}$. If at a stage Ω is approximated by $\Omega_q=\bigcup_{j=1}^{d'}\Omega_{q,j}$ (d' is not necessarily equal to the true number of objects d), and κ_i is approximated by a constant value $\kappa^j_{i,q}$ inside $\Omega_{q,j}$, then $D_T(\mathbf{x},\mathbb{R}^n\setminus\overline{\Omega}_q)$ is evaluated applying (22) with κ_i equal to

$$\kappa_{i,q}:=\begin{cases}\kappa_{i,0} & \text{in } \mathbb{R}^n\setminus\overline{\Omega}_q,\\ \kappa^j_{i,q} & \text{in } \Omega_{q,j}.\end{cases}$$

That is, in formula (22) κ_i is replaced by $\kappa_{i,0}$ and the diffusivity κ_i for the forward and adjoint fields is equal to $\kappa^j_{i,q}$ inside $\Omega_{q,j}$. □

4.3 General Problem with Two Unknown Parameters

In general, photothermal imaging involves transmission heat problems with the structure:

$$\begin{cases} U_t-\kappa_e\Delta U=0, & \text{in } \mathcal{R}\times(0,\infty),\\ U_t-\alpha_i\kappa_i\Delta U=0, & \text{in } \Omega\times(0,\infty),\\ U^- - U^+ = U_{inc}, & \text{on } \Gamma\times(0,\infty),\\ \alpha_i\partial_{\mathbf{n}}U^- - \partial_{\mathbf{n}}U^+ = \partial_{\mathbf{n}}U_{inc}, & \text{on } \Gamma\times(0,\infty),\\ \partial_{\mathbf{n}}U=0, & \text{on } \Pi\times(0,\infty),\\ U(\cdot,0)=0, & \text{in } \mathbb{R}^n_-. \end{cases} \tag{23}$$

The parameter $\alpha_i>0$ is the ratio of the interior and the exterior conductivities, and the interior diffusivity is written as $\alpha_i\kappa_i$. The problem described in Sect. 2 is a special case with $\alpha_i=1$. The variational reformulation contains an additional parameter: Find Ω, κ_i, α_i minimizing

$$J(\mathcal{R},\kappa_i,\alpha_i)=\frac{1}{2}\sum_{j=1}^{N} f(t_j)\int_{\Gamma_{meas}}\big(U_{total}(\mathbf{x},t_j) - U_{meas}(\mathbf{x},t_j)\big)^2 dl_{\mathbf{x}},$$

when $U_{total}(\mathbf{x},t)=U(\mathbf{x},t)+U_{inc}(\mathbf{x},t)\chi_{\mathcal{R}}(\mathbf{x})$, $U(\mathbf{x},t)$ being the solution of the extended forward problem (23).

The subsequent Laplace transformed and truncated functionals are updated accordingly. The Laplace transformed cost functional is approximated as

$$J(\mathcal{R},\kappa_i,\alpha_i):=\frac{1}{2}\sum_{j=1}^{N} f(t_j)\int_{\Gamma_{meas}}\left|\sum_{\ell=-m}^{m} c_\ell\, e^{s_\ell t_j} \times u_{total,s_\ell}(\mathbf{x};\kappa_i,\alpha_i) - U_{meas}(\mathbf{x},t_j)\right|^2 dl_{\mathbf{x}}, \tag{24}$$

where

$$u_{total,s_\ell}(\mathbf{x};\kappa_i,\alpha_i)=\begin{cases} u_{inc,s_\ell}(\mathbf{x})+u_{s_\ell}(\mathbf{x};\kappa_i,\alpha_i), & \text{in } \mathcal{R},\\ u_{s_\ell}(\mathbf{x};\kappa_i,\alpha_i), & \text{in } \Omega,\end{cases} \tag{25}$$

with $u_{inc,s_\ell}(\mathbf{x})=u_{inc}(\mathbf{x},s_\ell)$ defined in (7) and u_{s_ℓ} solving

$$\begin{cases} \Delta u_s+\lambda^2_{s,e}u_s=0, & \text{in } \mathcal{R},\\ \alpha_i\Delta u_s+\lambda^2_{s,i}u_s=0, & \text{in } \Omega,\\ u_s^- - u_s^+ = u_{inc,s}, & \text{on } \Gamma,\\ \alpha_i\partial_{\mathbf{n}}u_s^- - \partial_{\mathbf{n}}u_s^+ = \partial_{\mathbf{n}}u_{inc,s}, & \text{on } \Gamma,\\ \lim_{r\to\infty} r^{(n-1)/2}(\partial_r u_s-\imath\lambda_{s,e}u_s)=0, \end{cases} \tag{26}$$

with $\lambda^2_{s,e}:=-s/\kappa_e$, $\lambda^2_{s,i}:=-s/\kappa_i$, and $\mathcal{R}=\mathbb{R}^n_-\setminus\overline{\Omega}$.

To implement our scheme to identify parameters and domains we need a simpler expression for the topological derivative of this functional. The following formula was proved in [7].

Theorem 3 *When the parameters κ_i, α_i are fixed, the topological derivative of the cost functional (24) in $\mathbb{R}^n\setminus\overline{\Omega}$ is given by*

$$D_T\left(\mathbf{x},\mathbb{R}^n\setminus\overline{\Omega}\right) = \mathrm{Re}\left(\sum_{\ell=-m}^{m}\frac{n(1-\alpha_i)}{n-1+\alpha_i}\nabla u_{total,s_\ell}(\mathbf{x};\kappa_i,\alpha_i)\nabla p_{s_\ell}(\mathbf{x}) + \left(\frac{1}{\kappa_e}-\frac{1}{\kappa_i}\right)s_\ell u_{total,s_\ell}(\mathbf{x};\kappa_i,\alpha_i)\,p_{s_\ell}(\mathbf{x})\right), \tag{27}$$

where $p_{s_\ell} \in H^1(\mathbb{R}^n)$ *is a solution of the adjoint problem*

$$\begin{cases} \Delta p + \lambda^2_{s_\ell,e}\, p = B_\ell\, \delta_{\Gamma_{meas}}, & \text{in } \mathcal{R}, \\ \alpha_i \Delta p + \lambda^2_{s_\ell,i}\, p = 0, & \text{in } \Omega, \\ p^- - p^+ = 0, & \text{on } \Gamma, \\ \alpha_i \partial_{\mathbf{n}} p^- - \partial_{\mathbf{n}} p^+ = 0, & \text{on } \Gamma, \end{cases} \tag{28}$$

with $\lambda_{s_{\ell,e}} = -s_\ell/\kappa_e$, $\lambda_{s_{\ell,i}} = -s_\ell/\kappa_i$, *and*

$$B_\ell(\mathbf{x}) := \sum_{j=1}^{N} f(t_j) c_\ell e^{s_\ell t_j} \times \overline{\left(U_{meas}(\mathbf{x}, t_j) - \sum_{k=-m}^{m} c_k e^{s_k t_j} u_{total,s_k}(\mathbf{x}; \kappa_i, \alpha_i) \right)}.$$

The two parameters are updated using the following correctors for guesses of κ_i and α_i:

Theorem 4 *When* Ω *is fixed, the derivative with respect to* η *of the function* $J(\eta) = J(\mathcal{R}, \kappa_i + \eta\psi, \alpha_i + \eta\phi)$, J *defined in* (24), *evaluated at zero is*:

$$J'(0) = \mathrm{Re}\left(\sum_{\ell=-m}^{m} \int_\Omega \left(\frac{s_\ell}{\kappa_i^2}\, \psi\, u_{total,s_\ell}(\mathbf{x}; \kappa_i, \alpha_i)\, p_{s_\ell}(\mathbf{x}) - \phi\, \nabla u_{total,s_\ell}(\mathbf{x}; \kappa_i, \alpha_i) \nabla p_{s_\ell}(\mathbf{x}) \right) d\mathbf{x} \right),$$

where $p_{s_\ell} \in H^1(\mathbb{R}^n)$ *is a solution of* (28).

Proof We can follow step by step the proof of Theorem 1, replacing the sesquilinear form by:

$$\begin{aligned} & b(\eta, s; u, w) \\ & := \int_{\Omega_R} \left(\nabla u \nabla \overline{w} + \frac{s}{\kappa_e} u \overline{w} \right) d\mathbf{x} \\ & \quad + \int_\Omega \left((\alpha_i + \eta\phi) \nabla u \nabla \overline{w} + \frac{s}{\kappa_i + \eta\psi} u \overline{w} \right) d\mathbf{x} \\ & \quad - \int_{\Gamma_R} \big(L(s)u\big) \overline{w}\, dl. \end{aligned}$$

□

Given $\Omega = \bigcup_{j=1}^{d} \Omega_j$, we look for piecewise constant approximations of κ_i and α_i. We can improve guesses $\kappa^j_{i,q}, \alpha^j_{i,q}$ in each Ω_j as $\kappa^j_{i,q+1} = \kappa^j_{i,q} + \eta\psi_j$, $\alpha^j_{i,q+1} = \alpha^j_{i,q} + \eta\phi_j$ using the correctors:

$$\psi_j = -\,\mathrm{Re} \int_{\Omega_j} \left(\sum_{\ell=-m}^{m} s_\ell\, u_{total,s_\ell}\big(\mathbf{x}; (\kappa^1_{i,q}, \ldots, \kappa^d_{i,q}), (\alpha^1_{i,q}, \ldots, \alpha^d_{i,q})\big)\, p_{s_\ell}(\mathbf{x}) \right) d\mathbf{x},$$

$$\phi_j = \mathrm{Re} \int_{\Omega_j} \left(\sum_{\ell=-m}^{m} \nabla u_{total,s_\ell}\big(\mathbf{x}; (\kappa^1_{i,q}, \ldots, \kappa^d_{i,q}), (\alpha^1_{i,q}, \ldots, \alpha^d_{i,q})\big) \nabla p_{s_\ell}(\mathbf{x}) \right) d\mathbf{x},$$

with small $\eta > 0$. The forward and adjoint fields are computed for $\kappa_i = \kappa^j_{i,q}$ and $\alpha_i = \alpha^j_{i,q}$ inside each component Ω_j.

Remark We have used the non-standard formulation (23) of the general photothermal imaging problem, where α_i is the ratio between the interior and the exterior conductivities, κ_e is the exterior diffusivity and the interior diffusivity is written as $\alpha_i \kappa_i$. This notation simplifies the computation of topological derivatives. However it is rather simple to adapt the results in this paper to the more commonly used notation

$$\begin{cases} \rho_e U_t - \alpha_e \Delta U = 0, & \text{in } \mathcal{R} \times (0, \infty), \\ \rho_i U_t - \alpha_i \Delta U = 0, & \text{in } \Omega \times (0, \infty), \\ U^- - U^+ = U_{inc}, & \text{on } \Gamma \times (0, \infty), \\ \alpha_i \partial_{\mathbf{n}} U^- - \alpha_e \partial_{\mathbf{n}} U^+ = \alpha_e \partial_{\mathbf{n}} U_{inc}, & \text{on } \Gamma \times (0, \infty), \\ \partial_{\mathbf{n}} U = 0, & \text{on } \Pi \times (0, \infty), \\ U(\cdot, 0) = 0, & \text{in } \mathbb{R}^n_-, \end{cases}$$

where ρ_e, ρ_i are the mass densities of the materials multiplied by their specific heat capacity and α_e, α_i are the thermal conductivities (the thermal diffusivity is $\kappa = \alpha/\rho$).

5 Reconstructions for Thermal Waves

In this section we test the performance of our numerical method. First we consider the simpler problem of recovering the geometry of an object immersed in the half plane $\mathbb{R}^2_- = \{(x, y) \in \mathbb{R}^2,\ y < 0\}$ when its interior parameters are known. Next, we deal with the reconstruction of the defect and its diffusivity, assuming that the ratio between the conductivities $\alpha_i = 1$ is known. Afterwards we consider a geometrical configuration with two objects with unknown diffusivities, assuming that both materials have the same conductivity as the exterior media, that is, $\alpha_i = 1$. Finally we illustrate the ability of the method to recover the defect and the unknown parameters α_i, κ_i.

To compute an initial guess for the objects we set $\Omega = \emptyset$ and evaluate $D_T(\mathbf{x}, \mathbb{R}^2_-)$ on a grid of points. In this case the total field is known explicitly: $u_{total,s_\ell} = u_{inc,s_\ell}$ given by (7). In practice, Γ_{meas} is composed of a finite number of sampling points $\mathbf{x}_1, \ldots, \mathbf{x}_M$ and the solution to the adjoint problem (16) is given by

$$p_{s_\ell}(\mathbf{x}) = -\frac{\iota}{4} \sum_{k=1}^{M} \big(H_0^{(1)}(\lambda_{s_\ell} |\mathbf{x} - \mathbf{x}_k|) + H_0^{(1)}(\lambda_{s_\ell} |\widehat{\mathbf{x}} - \mathbf{x}_k|) \big) \times B_\ell(\mathbf{x}_k),$$

where $\widehat{\mathbf{x}} = (x, -y)$ is the reflected point of $\mathbf{x} = (x, y)$ with respect to $\Pi = \{(x, y) \in \mathbb{R}^2,\ y = 0\}$, and $H_0^{(1)}$ is the Hankel function of the first kind and order zero.

Scatterers are likely to be located in the regions where $D_T(\mathbf{x}, \mathbb{R}^2_-)$ attains large negative values. The computation of the initial guess is therefore extremely cheap. In the subsequent iterations $\Omega \neq \emptyset$ and the direct and adjoint problems have to be solved numerically for each s_ℓ. As we have already mentioned, the value $m = 10$ provides accurate approximations of $U(\mathbf{x}, t)$ using (11). By symmetry, we only have to solve 11 stationary forward and adjoint problems. The parameters λ^2 involved in these problems are complex valued and therefore we do not need to avoid Dirichlet eigenvalues of the Laplace operator. We use a simple boundary integral formulation based on single layer potentials that was proposed in [24]. For the discretization we apply a fully discrete version of a Galerkin method using the space of trigonometric polynomials (see [24] for details and [25] for other formulations and full discretizations).

We consider first the object Ω represented in Fig. 2 by a solid white line. Inside Ω the diffusivity is $\kappa_i = 1$. The diffusivity of the exterior matrix is $\kappa_e = 5$. Synthetic data $U_{meas}(\mathbf{x}, t)$ at Π were generated by solving the forward time dependent problem with a higher number of discretization points on Γ and a higher number of quadrature points for the time discretization. A 1 % relative random noise at each observation point was added to avoid inverse crimes.

We consider 6 incident waves generated at the uniformly distributed source points on Π represented in Fig. 2 by '•' marks. Measurements were taken at the 7 observation points on Π represented by '×' marks at 10 uniformly distributed times on the interval $[0.05, 0.5]$. The interested reader can find in [7] a gallery of numerical experiments discussing the accuracy of the method for known diffusivities when changing the number of observation points, source points and/or time instants of observation. A small number of sampling points and of incident fields allows for good reconstructions when many time measurements are available.

Let us start by computing the topological derivative when $\Omega = \emptyset$ for the following weight functions:

$$f_1(t) = \max_{\mathbf{x}\in\{\mathbf{x}_1,\ldots,\mathbf{x}_M\}} \left|U_{meas}(\mathbf{x}, t)\right|^{-1}, \tag{29}$$

$$f_2(t) = \max_{\mathbf{x}\in\{\mathbf{x}_1,\ldots,\mathbf{x}_M\}} \left|U_{inc}(\mathbf{x}, t)\right|^{-1}, \tag{30}$$

$$f_3(t) = \max_{\mathbf{x}\in\{\mathbf{x}_1,\ldots,\mathbf{x}_M\}} \left|U_{meas}(\mathbf{x}, t)\right|^{-2}, \tag{31}$$

$$f_4(t) = \max_{\mathbf{x}\in\{\mathbf{x}_1,\ldots,\mathbf{x}_M\}} \left|U_{inc}(\mathbf{x}, t)\right|^{-2}. \tag{32}$$

The values of these derivatives at the sampling region $[-3, 3] \times [-2.5, 0]$ are shown in Fig. 2. Observing the larger negative values of the topological derivative we get reasonable information about the number of defects and their location in all the cases. Notice that f_1 and f_2 detect the regions of Ω close to the observation points while f_3 and f_4 are better to locate the center of Ω.

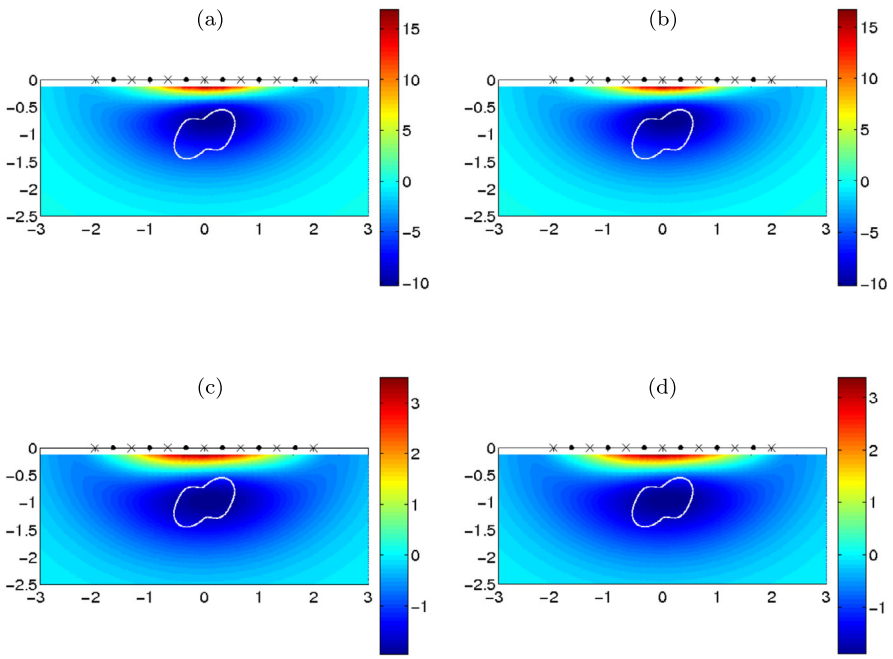

Fig. 2 Topological derivative when $\Omega = \emptyset$ and κ_i is known for the weight functions defined in (29)–(32): (**a**) $f = f_1$, (**b**) $f = f_2$, (**c**) $f = f_3$, (**d**) $f = f_4$ (Color figure online)

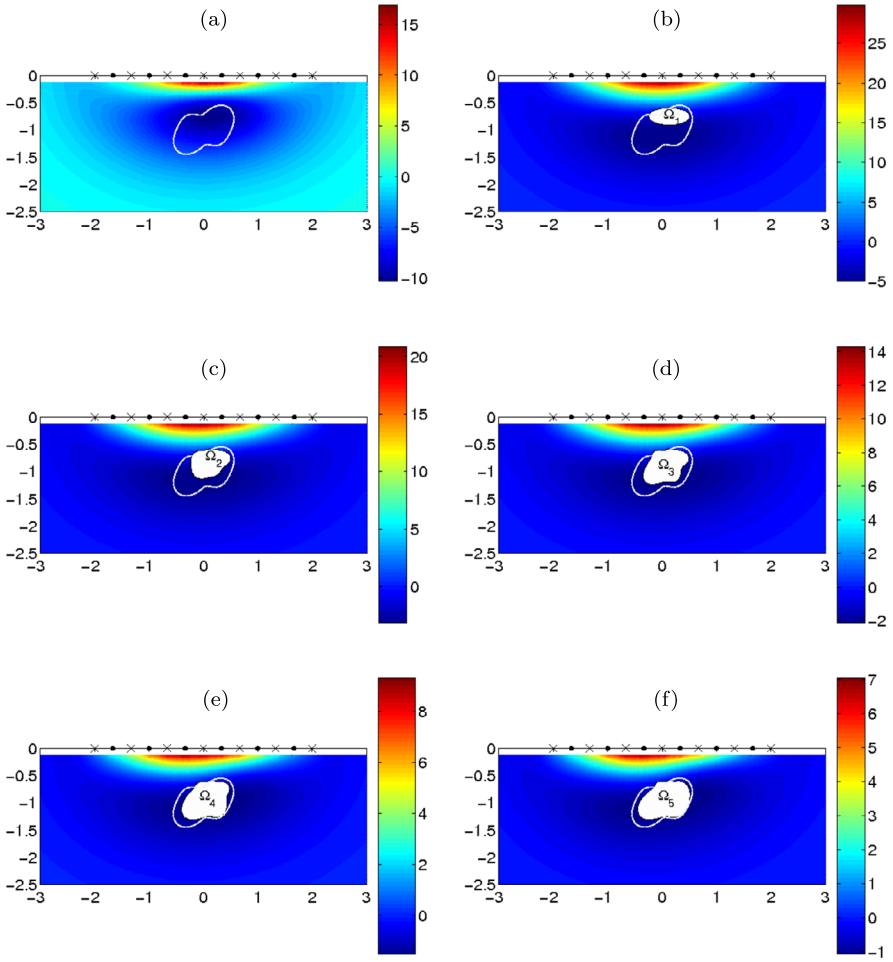

Fig. 3 First steps of the iterative method when κ_i is known and $f = f_1$: (**a**) Topological derivative when $\Omega = \emptyset$. (**b**)–(**d**) Approximate domain Ω_q superimposed to the topological derivative for $\Omega = \Omega_q$, $q = 1, \ldots, 5$ (Color figure online)

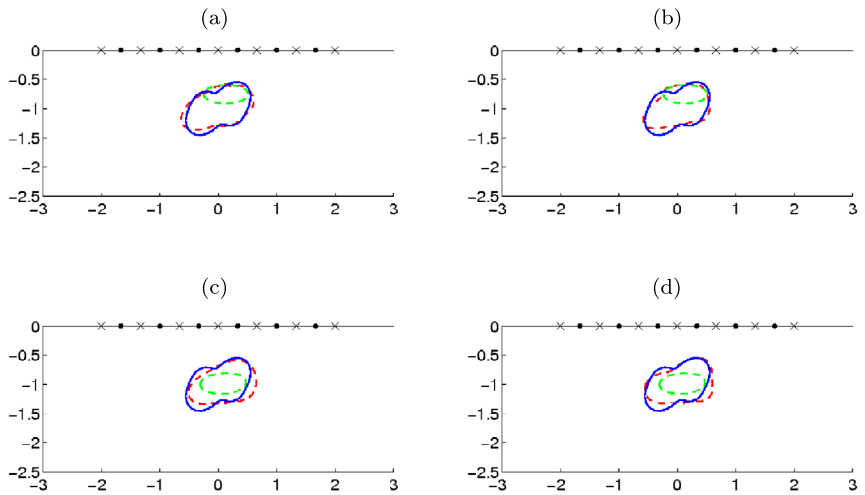

Fig. 4 Initial guess (*green dashed line*) and predicted object (*red dashed line*) for different weight functions: (**a**) $f = f_1$, (**b**) $f = f_2$, (**c**) $f = f_3$, (**d**) $f = f_4$ (Color figure online)

In Fig. 3 we apply the monotone iterative method (19) for the weight function f_1. The initial guess Ω_1 is selected as the region where $D_T(\mathbf{x}, \mathbb{R}^2_-)$ attains the larger negative values. In the next step Ω_2 is defined by adding to Ω_1 the points where $D_T(\mathbf{x}, \mathbb{R}^2_- \setminus \overline{\Omega_1})$ is large and negative and so on. We observe that Ω_1 is improved in a very few steps. The algorithm stopped at the ninth iteration. The reconstructed object is shown in Fig. 4(a).

Figure 4 shows the initial guess and the final predicted object when applying the method for the selected weight functions. f_1 provides almost the same reconstruction as f_2. The same happens with f_3 and f_4. In the four cases we ob-

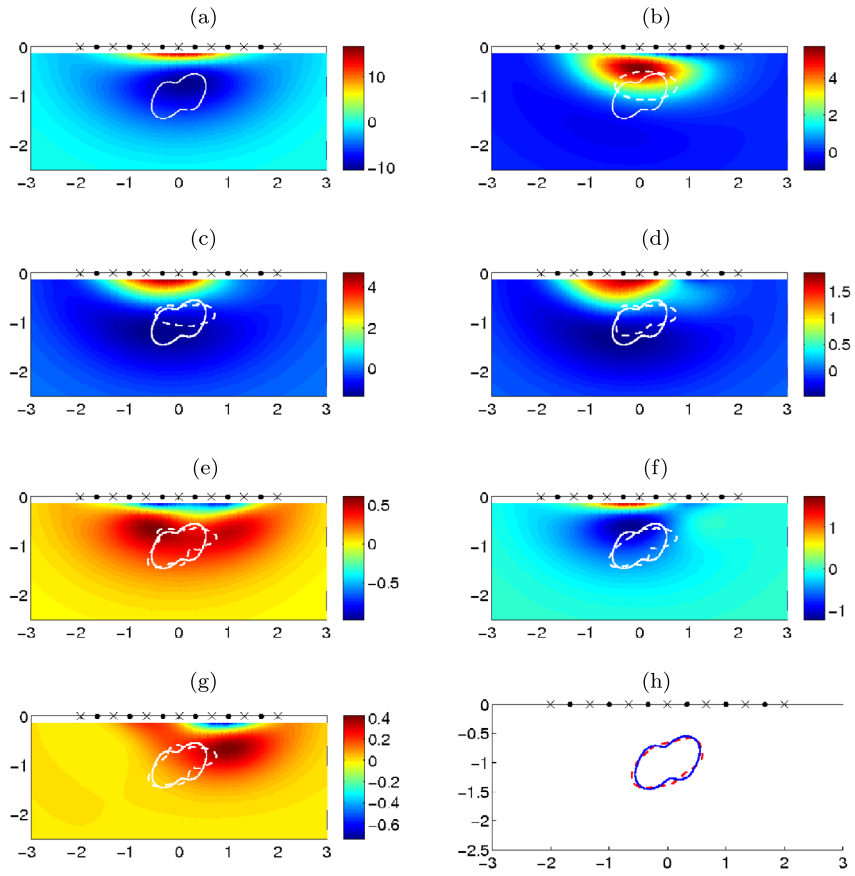

Fig. 5 Performance of the non-monotone method (21) for $f = f_1$: (**a**) Topological derivative when $\Omega = \emptyset$. (**b**)–(**g**) Approximate domain Ω_q (*dashed line*) and topological derivative when $\Omega = \Omega_q$, for $q = 1, \ldots, 6$. (**h**) Final reconstruction (Color figure online)

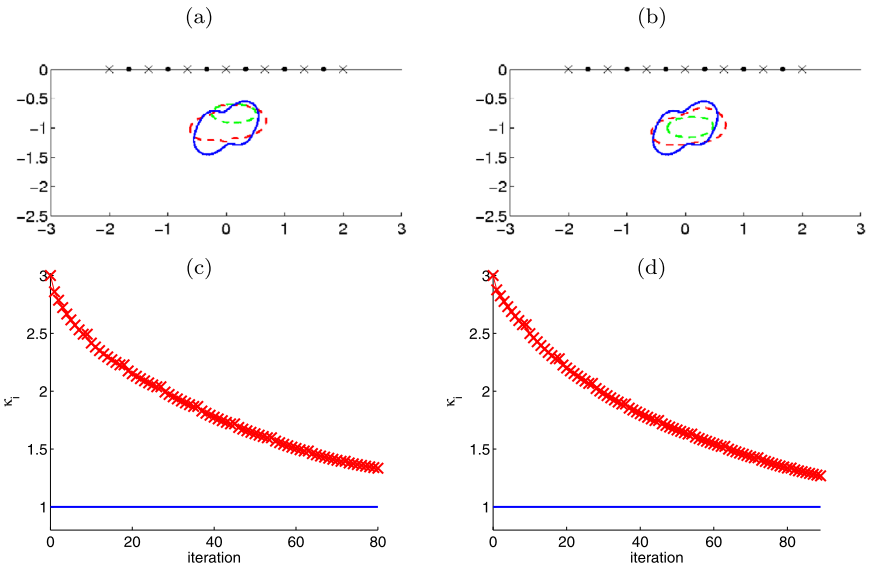

Fig. 6 Reconstructions with the hybrid method: (**a**) Initial guess (*green dashed line*) and predicted object (*red dashed line*) when $f = f_1$. (**b**) Initial guess (*green dashed line*) and predicted object (*red dashed line*) when $f = f_3$. (**c**) Values of κ_i versus the number of iterations when $f = f_1$. (**d**) Values of κ_i versus the number of iterations when $f = f_3$ (Color figure online)

tain reasonable reconstructions in few iterations (9 for f_1, f_2 and f_3, and 10 for f_4). Notice that we are not only able to reconstruct the "heated" part of the object (the region close to the observation points), as happens when considering time–harmonic excitations [7], but also the "unheated" region.

In all the previous reconstructions, the constant C_q appearing in (19) was taken as the minimum value of the topological derivative multiplied by $\delta_1 = 0.85$ for C_1, and by $\delta_q = 0.9$ for $q \geq 2$. As expected, the selection of these thresholds affects the reconstruction. Choosing $\delta_1 = 0.75$ instead of $\delta_1 = 0.85$, the initial guess for $f = f_1$ is the object represented by a dashed line in Fig. 5(b), which includes many spurious points. If we observe the values of the topological derivative computed when $\Omega = \Omega_1$, we notice a big

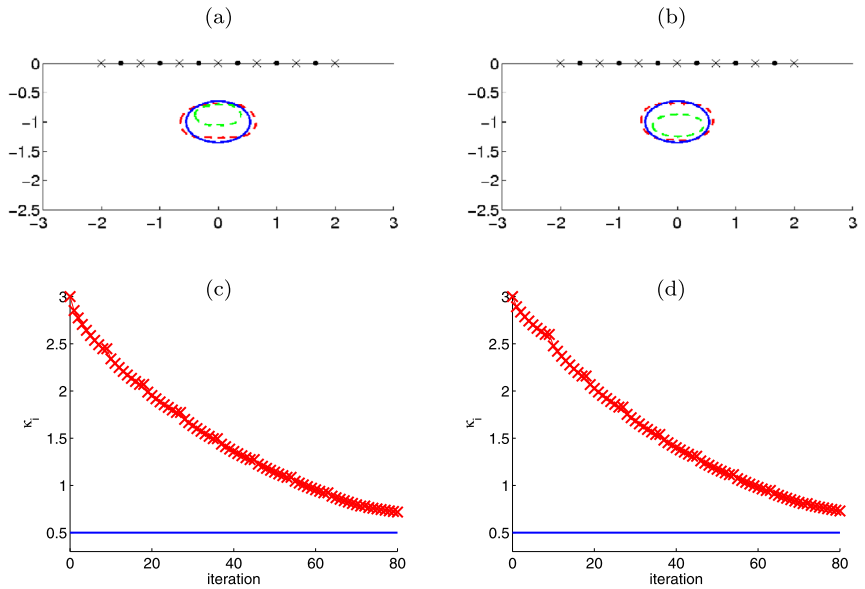

Fig. 7 Reconstructions with the hybrid method: (**a**) Initial guess (*green dashed line*) and predicted object (*red dashed line*) when $f = f_1$. (**b**) Initial guess (*green dashed line*) and predicted object (*red dashed line*) when $f = f_3$. (**c**) Values of κ_i versus the number of iterations when $f = f_1$. (**d**) Values of κ_i versus the number of iterations when $f = f_3$ (Color figure online)

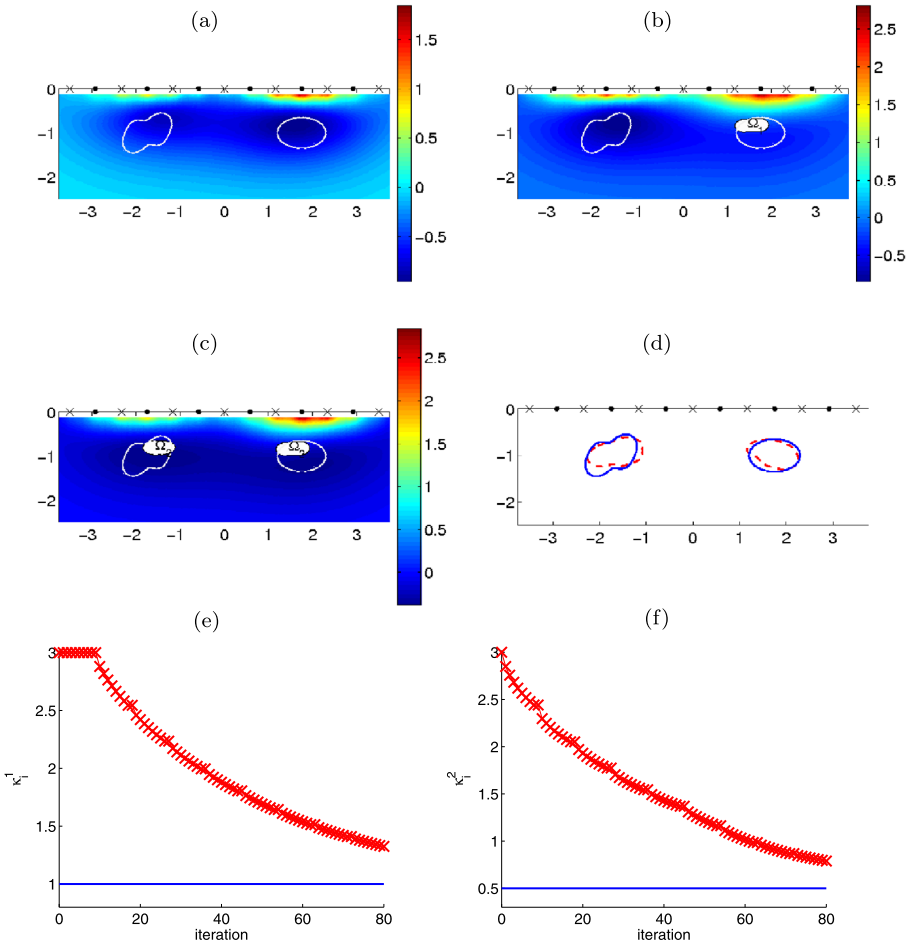

Fig. 8 Performance of the hybrid method in a configuration with two objects when $f = f_1$: (**a**) Topological derivative when $\Omega = \emptyset$. (**b**)–(**c**) Approximate domains Ω_q superimposed to the topological derivative for $\Omega = \Omega_q$, $q = 1, 2$. (**d**) Final reconstruction of the defects (*red dashed line*). (**e**) Values of κ_i^1 versus the number of iterations. (**f**) Values of κ_i^2 versus the number of iterations (Color figure online)

region at the top of the object where the derivative attains large positive values, indicating that C_1 should be increased. The monotone algorithm (19) without correcting C_1 would fail. Using the non-monotone algorithm (21) we can remove spurious points (those inside the object where the topological derivative is large and positive). The next iteration using this method is given in Fig. 5(c). The reconstructed object is represented by a dashed line. The computation of the topo-

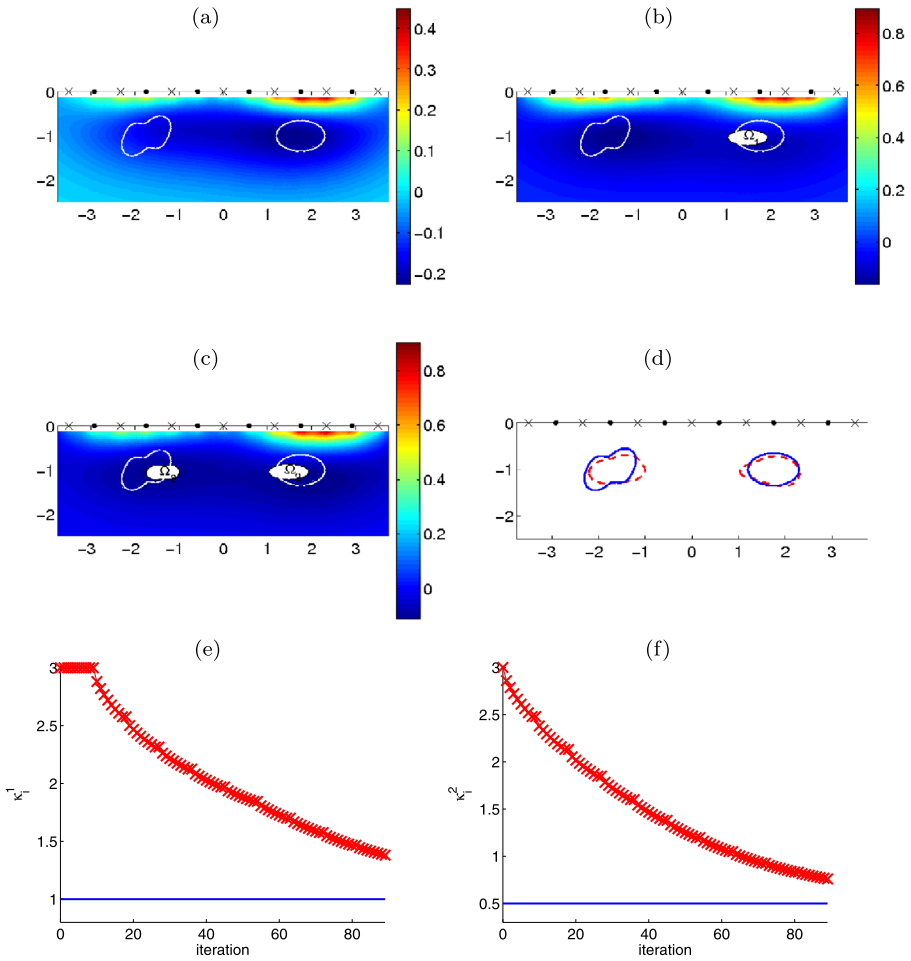

Fig. 9 Performance of the hybrid method in a configuration with two objects when $f = f_3$: (**a**) Topological derivative when $\Omega = \emptyset$. (**b**)–(**c**) Approximate domains Ω_q superimposed to the topological derivative for $\Omega = \Omega_q$, $q = 1, 2$. (**d**) Final reconstruction of the defects (*red dashed line*). (**e**) Values of κ_i^1 versus the number of iterations. (**f**) Values of κ_i^2 versus the number of iterations (Color figure online)

logical derivative for this object indicates now that we have to add new points to the current approximation. No spurious points inside the object are detected. The same happens at the next iteration, see Fig. 5(d). Some spurious points are detected in the next iteration, as observed in Fig. 5(e). After 12 iterations with the non-monotone algorithm we obtained the final reconstruction given in Fig. 5(h). The quality of the final reconstruction using the monotone method (with well calibrated constants) and with the non-monotone method is similar, compare Fig. 4(a) with Fig. 5(h). For simplicity we will use the monotone method in the sequel with initial constants $\delta_1 = 0.85$ and $\delta_q = 0.9$ for $q \geq 2$. If at some iteration many points near the boundary of the current approximation where the topological derivative attains large positive values appear, then one has to use the non-monotone method to remove spurious regions, or to increase the constant δ_k in the previous step. The non-monotone method is unavoidable when dealing with annular defects (see [6] for a reconstruction of an annular object in an acoustic setting).

Let us discuss now the ability of the hybrid topological derivative-gradient based method to recover the geometry of the object as well as its diffusivity κ_i, when $\alpha_i = 1$ is known. We start the algorithm with initial guess $\kappa_{i,0} = 3$. To obtain an initial guess for the domain we set $\Omega = \emptyset$ and compute $D_T(\mathbf{x}, \mathbb{R}^2_-)$. When $\Omega = \emptyset$ the functions u_{total,s_ℓ} and p_{s_ℓ} appearing in (22) do not depend on κ_i. Therefore the topological derivative when $\kappa_i = \kappa_{i,0}$ is equal to its counterpart for the true $\kappa_i = 1$ (represented in Fig. 2) except for the scale (we have now the multiplying factor $(1/\kappa_e - 1/\kappa_{i,0})$ instead of $(1/\kappa_e - 1/\kappa_i)$). The initial guesses for $f = f_1$ and $f = f_3$ are represented by green dashed lines in Figs. 6(a, b). They are exactly the same as in Figs. 4(a, c), obtained for the true value κ_i. Once the starting parameter and object are set, we alternate eight iterations with the gradient method to improve the value of the diffusivity (fixing the current object) with one topological derivative computation to update the domain (fixing the value of κ_i). The hybrid algorithm stopped at the ninth iteration with respect to the domain when $f = f_1$ and at the tenth iteration when $f = f_3$. The final reconstructed objects are represented in Figs. 6(a, b) by red dashed lines. The values of κ_i throughout the iterations are given in Figs. 6(c, d). Two identical values of $k_{i,q}$ (iterations $q = 9, 18, 27, \ldots$ in the plots) mark each iteration to improve the domains since the parameter is not updated. The final approximate diffusivities were 1.33 for f_1 and 1.27 for f_3.

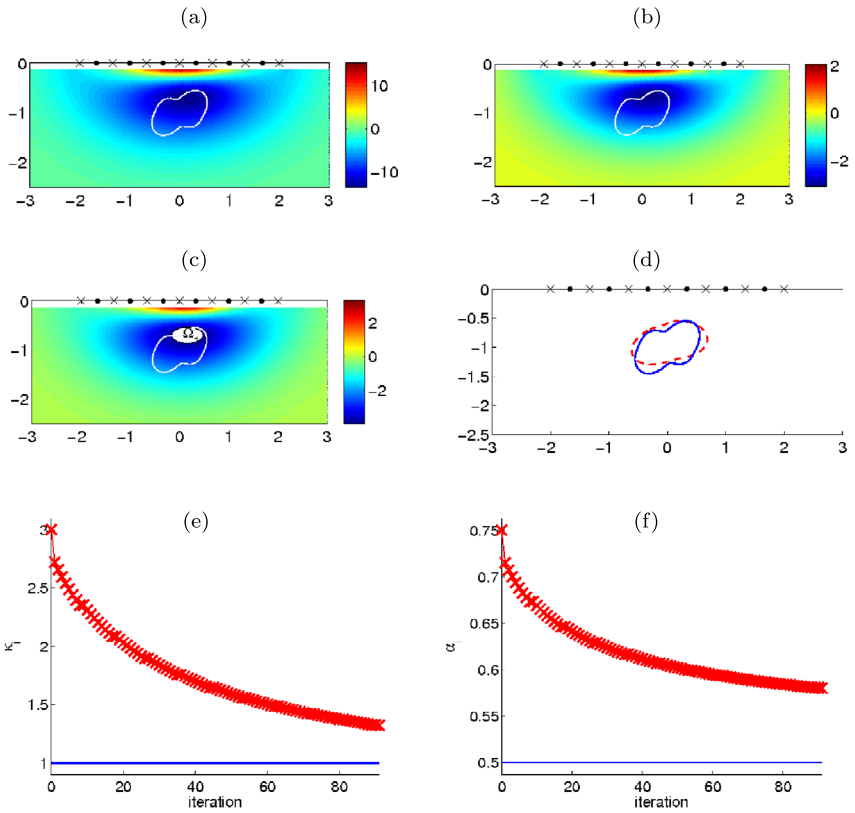

Fig. 10 Performance of the hybrid method when κ_i and α_i are unknown for $f = f_1$: (**a**) Topological derivative when $\Omega = \emptyset$ and $\kappa_i = 1$, $\alpha_i = 0.5$ (true parameters). (**b**) Topological derivative when $\Omega = \emptyset$ and $\kappa_i = \kappa_{i,0} = 3$, $\alpha_i = \alpha_{i,0} = 0.75$ (initial guesses). (**c**) Approximated domain Ω_1 superimposed to the topological derivative for $\Omega = \Omega_1$, $\kappa_i = \kappa_{i,9} = 2.35$ and $\alpha_i = \alpha_{i,9} = 0.67$. (**d**) Predicted (*red dashed line*) and true (*blue solid line*) objects. (**e**) Values of κ_i versus the number of iterations. (**f**) Values of α_i versus the number of iterations (Color figure online)

Figure 7 is the counterpart of Fig. 6 for an ellipse with diffusivity $\kappa_i = 0.5$. The exterior parameter was again $\kappa_e = 5$. The value of the approximated diffusivity is 0.72 for f_1 and 0.73 for f_3.

In the next example we test the algorithm in a configuration with two defects. The left object has diffusivity $\kappa_i^1 = 1$ and the right one $\kappa_i^2 = 0.5$. In the exterior matrix $\kappa_e = 5$. We initialize the algorithm choosing $\kappa_{i,0} = 3$. Then we compute $D_T(\mathbf{x}, \mathbb{R}^2_-)$ for the weight function f_1 (see Fig. 8(a)) to select the initial guess Ω_1 represented in Fig. 8(b). The topological derivative only detects the rightmost object. The initial guess has only one defect. We perform eight iterations with respect to the parameter to update the approximation of κ_i^2. The left object was missed and therefore κ_i^1 is equal to $\kappa_{i,0}$ during the first application of the gradient method, see Fig. 8(e). In the next step we fix the value of the parameter and compute the topological derivative when $\Omega = \Omega_1$. The leftmost defect is detected now as shown in Figs. 8(b, c). We apply now the gradient method to update the parameter values using (17). Next we update the domains and so on. The reconstructions of the defects are shown in Fig. 8(d). The values of the parameters throughout the iterative procedure are given in Figs. 8(e, f). In Fig. 9 we repeated the experiment choosing $f = f_3$. For both weight functions we obtained again satisfactory reconstructions with few data in a small number of iterations. It is remarkable that the quality of the reconstruction of the objects and of their parameters is almost the same as when the defects are alone (compare Figs. 8 and 9 with Figs. 6 and 7).

To end this section we consider the problem of recovering an object in the general setting, when both parameters $\kappa_i = 1$ and $\alpha_i = 0.5$ are unknown. The exterior diffusivity is $\kappa_e = 5$ as before. We start the hybrid method with initial values $\kappa_{i,0} = 3$ and $\alpha_{i,0} = 0.75$. Notice that in the simplified case with $\alpha_i = 1$, the points where the topological derivative (22) attains the largest negative values do not depend on the initial guess for κ_i. This parameter only appears as a multiplying factor, and we obtain exactly the same region as when using the true parameter. However, when dealing with the full problem with two unknown parameters κ_i and α_i, formula (27) does depend on the initial guesses. This fact is illustrated in Figs. 10(a, b). In (a) we represent the values of the topological derivative obtained when $\Omega = \emptyset$ and $\kappa_i = 1$, $\alpha_i = 0.5$ are the true parameters, and (b) is its counterpart for $\kappa_i = \kappa_{i,0} = 3$ and $\alpha_i = \alpha_{i,0} = 0.75$. Our initial guess for the domain is represented in Fig. 10(c). After eight iterations of the gradient method to approximate the parameters we obtain the values $\kappa_{i,9} = 2.35$ and $\alpha_{i,9} = 0.67$. These are the values used to compute now the topological derivative (27) for $\Omega = \Omega_1$, shown in Fig. 10(c). In the next plot we represent our final reconstruction of the object. The quality of the reconstruction is slightly better than when $\alpha_i = 1$ (compare with Fig. 6(a)). The final approximations of the parameters are $\kappa_i = 1.32$ and $\alpha_i = 0.58$. Their values versus the number

of iterations are given in Figs. 10(d, e). We have obtained a similar value for κ_i as when we applied the method with $\alpha_i = 1$ (assumed to be known).

6 Conclusions

We have presented a technique to reconstruct multiple objects buried near a surface and identify their material parameters by scattering of pulse–like thermal waves. The inverse problem is reformulated as a constrained optimization problem, with a time dependent transmission problem for the heat equation acting as the constraint. The geometry of the domains and their parameters are the design variables. The original optimization problem is Laplace transformed and then conveniently truncated to produce an approximated optimization problem with a finite number of stationary constraints. Approximations for the objects and their material parameters are obtained by a descent method. Guesses and approximations for the domains are found by topological derivative techniques. Improved corrections for their parameters are generated by gradient methods. Numerical tests illustrate the good performance of the technique with just a few iterations. We have focussed on piecewise constant material parameters. Smoothly varying coefficients can be dealt with as in [6, 8].

Acknowledgements The authors are partially supported by the Spanish Government research project TRA2010–18054 and the Spanish Ministerio de Economia y Competitividad Grants No. FIS2011-28838-C02-02, and No. FIS2010-22438-E.

References

1. Allaire, G., de Gournay, F., Jouve, F., Toader, A.M.: Structural optimization using topological and shape sensitivity via a level-set method. Control Cybern. **34**, 59–80 (2005)
2. Almond, D.P., Patel, P.M.: Photothermal Science and Techniques. Chapman and Hall, London (1996)
3. Banks, H.T., Kojima, F.: Boundary shape identification problems in two-dimensional domains related to thermal testing of materials. Q. Appl. Math. **47**, 273–293 (1989)
4. Banks, H.T., Kojima, F., Winfree, W.P.: Boundary estimation problems arising in thermal tomography. Inverse Probl. **6**, 897–921 (1990)
5. Cakoni, F., Colton, D., Monk, P.: The determination of the surface conductivity of a partially coated dielectric. SIAM J. Appl. Math. **65**, 767–789 (2005)
6. Carpio, A., Rapún, M.-L.: Solving inverse inhomogeneous problems by topological derivative methods. Inverse Probl. **24**, 045014 (2008)
7. Carpio, A., Rapún, M.-L.: Domain reconstruction by photothermal techniques. J. Comput. Phys. **227**, 8083–8106 (2008)
8. Carpio, A., Rapún, M.-L.: Hybrid topological derivative and gradient based methods for electrical impedance tomography. Inverse Probl. **28**, 095010 (2012)
9. Costabel, M., Stephan, E.: A direct boundary integral equation method for transmission problems. J. Math. Anal. Appl. **106**, 367–413 (1985)
10. Elden, L., Berntsson, F., Reginska, T.: Wavelet and Fourier methods for solving the sideways heat equation. SIAM J. Sci. Comput. **21**, 2187–2205 (2000)
11. Feijoo, G.R.: A new method in inverse scattering based on the topological derivative. Inverse Probl. **20**, 1819–1840 (2004)
12. Garrido, F., Salazar, A.: Thermal wave scattering from spheres. J. Appl. Phys. **95**, 140–149 (2004)
13. Guzina, B.B., Bonnet, M.: Small-inclusion asymptotic of misfit functionals for inverse problems in acoustics. Inverse Probl. **22**, 1761–1785 (2006)
14. Guzina, B.B., Chikichev, I.: From imaging to material identification: a generalized concept of topological sensitivity. J. Mech. Phys. Solids **55**, 245–279 (2007)
15. Heath, D.M., Welch, C.S., Winfree, W.P.: Quantitative thermal diffusivity measurements of composites. In: Review of Progress in Quantitative Non-Destructive Evaluation, vol. 5B, pp. 1125–1132. Plenum, New York (1986)
16. Hohage, T., Rapún, M.-L., Sayas, F.-J.: Detecting corrosion using thermal measurements. Inverse Probl. **23**, 53–72 (2007)
17. Hohage, T., Sayas, F.-J.: Numerical approximation of a heat diffusion problem by boundary element methods using the Laplace transform. Numer. Math. **102**, 67–92 (2005)
18. Isakov, V.: Inverse Problems for Partial Differential Equations. Springer, New York (1998)
19. López-Fernández, M., Palencia, C.: On the numerical inversion of the Laplace transform of certain holomorphic mappings. Appl. Numer. Math. **51**, 289–303 (2004)
20. Mandelis, A.: Diffusion-Wave Fields. Mathematical Methods and Green Functions. Springer, New York (2001)
21. Mandelis, A.: Diffusion waves and their uses. Phys. Today **53**, 29–34 (2000)
22. Nicolaides, L., Mandelis, A.: Image-enhanced thermal-wave slice diffraction tomography with numerically simulated reconstructions. Inverse Probl. **13**, 1393–1412 (1997)
23. Ocáriz, A., Sánchez-Lavega, A., Salazar, A.: Photothermal study of subsurface cylindrical structures II. Experimental results. J. Appl. Phys. **81**, 7561–7566 (1997)
24. Rapún, M.-L., Sayas, F.-J.: Boundary integral approximation of a heat diffusion problem in time-harmonic regime. Numer. Algorithms **41**, 127–160 (2006)
25. Rapún, M.-L., Sayas, F.-J.: Boundary element simulation of thermal waves. Arch. Comput. Methods Eng. **14**, 3–46 (2007)
26. Salazar, A., Sánchez-Lavega, A., Celorrio, R.: Scattering of cylindrical thermal waves in fiber composites: in-plane thermal diffusivity. J. Appl. Phys. **93**, 4536–4542 (2003)
27. Terrón, J.M., Salazar, A., Sánchez-Lavega, A.: General solution for the thermal wave scattering in fiber composites. J. Appl. Phys. **91**, 1087–1098 (2002)

A. Carpio is Professor of Applied Mathematics at the Universidad Complutense de Madrid. She received her Ph.D. degree at the Laboratorie Jacques Louis Lions (Université, Paris VI, 1993) and conducted her postdoctoral research at the Oxford Centre for Industrial and Applied Mathematics (University of Oxford, 1996–1997). Her research interests include inverse problems and variational methods for image analysis, shape reconstruction and parameter identification.

M.-L. Rapún received her Ph.D. degree in Applied Mathematics from the Universidad de Zaragoza (Spain) in 2004. She is Associate Professor at the School of Aeronautical Engineering, Universidad Politécnica de Madrid (Spain). Her research interests include boundary element methods and their applications, direct and inverse problems of scattering of acoustic and thermal waves, and reduced order methods.